

Thermal Analysis and Design of AlGaInP-based Light Emitting Diode Arrays

Zhang Ban^{1,2}, Zhongzhu Liang^{1*}, Jingqiu Liang¹, Weibiao Wang¹, JinguangLv¹, and Yuxin Qin¹

¹State Key Laboratory of Applied Optics, Changchun Institute of Optics, Fine Mechanics and Physics,
Chinese Academy of Sciences, Changchun, Jilin 130033, China

²University of Chinese Academy of Sciences, Beijing 100039, China

(Received June 28, 2016 : revised November 8, 2016 : accepted April 3, 2017)

LED arrays with pixel numbers of 3×3 , 4×4 , and 5×5 have been studied in this paper in order to enhance the optical output power and decrease heat dissipation of an AlGaInP-based light emitting diode display device (pixel size of $280\times 280\text{ }\mu\text{m}$) fabricated by micro-opto-electro-mechanical systems. Simulation results showed that the thermal resistances of the 3×3 , 4×4 , 5×5 arrays were 52°C/W , 69.7°C/W , and 84.3°C/W . The junction temperature was calculated by the peak wavelength shift method, which showed that the maximum value appears at the center pixel due to thermal crosstalk from neighboring pixels. The central temperature would be minimized with $40\text{ }\mu\text{m}$ pixel pitch and $150\text{ }\mu\text{m}$ substrate thickness as calculated by thermal modeling using finite element analysis. The modeling can be used to optimize parameters of highly integrated AlGaInP-based LED arrays fabricated by micro-opto-electro-mechanical systems technology.

Keywords : AlGaInP LED array, Junction temperature, Thermal analysis

OCIS codes : (220.0220) Optical design and fabrication; (220.4000) Microstructure fabrication; (230.0230) Optical devices; (230.3670) Light-emitting diodes

I. INTRODUCTION

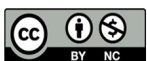
LEDs play important roles in many areas such as communications, lighting, and displays owing to their high brightness, low working voltage, fast response speed, and long working life [1-6]. Compared with a single LED with large size, an LED array has advantages of less significant current crowding effect, more uniform injection current, high optical output power, and reduced self-heating. Self-heating can increase non-radiative recombination, reduce optical output power and decrease lifetime, substantively impeding LED applications [7-10]. The basic ways to accelerate heat dissipation in high power LEDs include the addition of heat sinks and improvement of air convection. Moreover, some reports have shown that meshing large size chips into multi-chips is beneficial for the extraction of heat and light [6]. Heat dissipation can also be improved by reducing the substrate thickness or mounting the chip substrate with high thermal conductivity [11]. Recently, we reported a new fabrication method based on the Micro-Opto-Electro-Mechanical

Systems (MOEMS) integrated technique that was used to efficiently fabricate micro LED arrays [12-13]. However, a detailed study of the thermal characteristics of the LED array fabricated by this method has not been performed. Studies showed that the junction temperature increased and the thermal characteristics created by thermal crosstalk existed in the array. Hence, for LED array applications, it is necessary to effectively extract the heat generated in the LEDs during operation by adopting a suitable separation distance and substrate thickness [9].

In this paper, we introduce a new fabrication method and investigate thermal, electrical, and optical properties of a single LED pixel with 3×3 , 4×4 , and 5×5 LED arrays. The junction temperature was calculated using the peak wavelength shift method [14]. Also, the thermal resistance of LED arrays was calculated. Meanwhile, a finite element method was used to model the thermal characteristics of a 3×3 LED array. The calculations showed that the junction temperature of the center pixel is maximum owing to thermal crosstalk from neighboring pixels. The substrate thickness and pixel

*Corresponding author: liangzz@ciomp.ac.cn

Color versions of one or more of the figures in this paper are available online.



This is an Open Access article distributed under the terms of the Creative Commons Attribution Non-Commercial License (<http://creativecommons.org/licenses/by-nc/4.0/>) which permits unrestricted non-commercial use, distribution, and reproduction in any medium, provided the original work is properly cited.

separation pitch were then optimized by thermal analysis to enhance heat dissipation of LED arrays.

II. EXPERIMENT AND THERMAL MODELING

2.1 Materials and Fabrication

Metal-organic chemical vapor deposition (MOCVD) was used to grow the LED epitaxial wafer consisting of a GaAs substrate (350 μm), a GaP buffer layer (2 μm), a distributed Bragg Reflectors (DBRs) layer (700 nm), an AlInP:Mg electron blocking layer (500 nm), GaInP/AlGaInP multiquantum wells (MQWs), an AlInP:Si hole blocking layer (100 nm), and a GaP window layer (8 μm). The structure of the AlGaInP-based LED is shown in Fig. 1(a).

The specific technological processes based on MOEMS to fabricate the AlGaInP-based LED array were as follows. First, the LED wafer was grooved by an inductively coupled

plasma (ICP) etching technique with a SiO_2 mask, in order to make the grooves completely cut to the GaAs substrate. Figure 1(b) shows the surface morphology of the LED array after grooving. Then, the grooves were filled with polyimide in order to isolate each pixel. After that, positive ohmic contacts were fabricated as shown in Fig. 1(c) and an epoxy resin protection layer was added. After thinning the GaAs substrate, n-electrode was deposited and formed. Figure 1(d) shows a completed 5×5 LED array [12-13].

2.2 Measurement and Theoretical Basis

Figure 2 shows the schematic diagram of the test system. The emission spectrum and optical output power of the array were tested under different injection current and heat-sink temperature conditions. The junction temperature was obtained by calculating the wavelength peak shift of the emission spectrum.

The main way to dissipate heat for this device is heat conduction. In the heat conduction process, the temperature changes with time until the steady state is reached. Previous studies indicated that the chip reached the steady state when the duration of injected current was more than 100 ms [8]. Therefore, the steady-state model is selected here. Assuming that the thermal parameters of each layer in the LED are constant, the volume of the heat source is equal to the volume of the multiple quantum wells layer, the heat distribution generated by each multiple quantum wells layer is uniform, and we set heatsink temperature to 30 $^{\circ}\text{C}$.

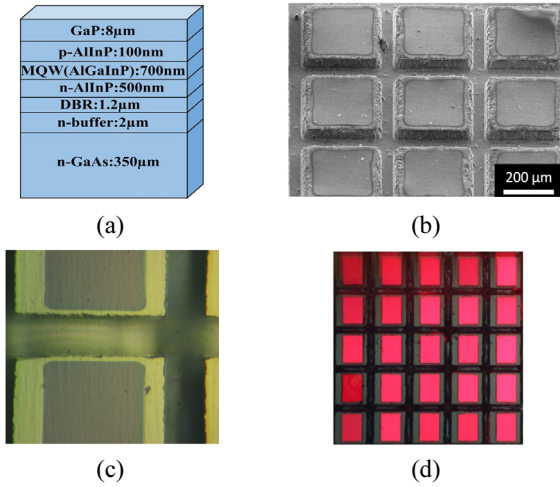


FIG. 1. (a) Schematic of the LED layer structure; (b) SEM imaging of the surface morphology of the LED array after ICP etching; (c) Surface of the anode after fabricating n-contacts; (d) 5×5 LED array during operation.

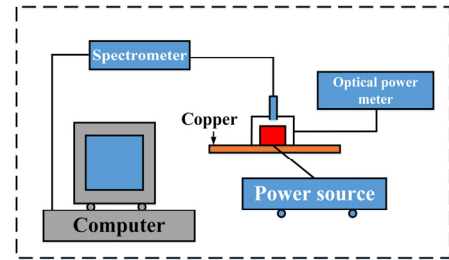


FIG. 2. The schematic diagram of the testing system.

TABLE 1. Thermal conductivities of the constituent materials for AlGaInP LEDs at 30 $^{\circ}\text{C}$

| Name | Material | Thickness | Thermal conductivity($\text{W/m} \cdot \text{k}$) |
|------------------|-------------|-------------------|---|
| p-Electrode | Au/AuCr | 100 nm | 315 |
| p-Window | GaP | 8 μm | 77 |
| p-Cladding layer | AlInP | 100 nm | 8 |
| MQWs | AlGaInP | 700 nm | $K_L=10.2$ $K_V=8.2$ |
| n-Cladding layer | AlInP | 500 nm | 6 |
| n-DBRs | AlAs/AlGaAs | 1.2 μm | $K_L=53.6$ $K_V=20.3$ |
| n-Buffer layer | GaP | 2 μm | 8 |
| n-Substrate | GaAs | 350 μm | 44 |
| n-Electrode | Au/AuCr | 100 nm | 315 |
| Heatsink | Cu | - | 400 |

Because the heat flux distribution is consistent in each direction, the three-dimensional steady heat conduction can be modelled using the Laplace's equation [15],

$$-k\left(\frac{\partial^2 T}{\partial x^2} + \frac{\partial^2 T}{\partial y^2} + \frac{\partial^2 T}{\partial z^2}\right) = Q \quad (1)$$

where Q represents the heat source density, T represents the temperature of each point, k represents the thermal conductivity of the constituent material. According to the definition of heat source density [11],

$$Q = \frac{P_{in}}{V_{MQW}} \quad (2)$$

where P_{in} represents dissipated heat power, V_{MQW} represents heat source volume.

According to the energy conservation law,

$$P_{in} = I \cdot U_F - P_o \quad (3)$$

where I represents injection current, U_F represents forward voltage, P_o represents optical output power.

In addition, each layer's temperature distribution is continuous, and the temperature continuity equation is satisfied at the junction area of any two layers [15-17]:

$$T_i(x, y, z_i) = T_{i+1}(x, y, z_i) \quad (4)$$

And

$$k_i \left. \frac{\partial T_1}{\partial z} \right|_{z=z_i} = k_{i+1} \left. \frac{\partial T_2}{\partial z} \right|_{z=z_i} \quad (5)$$

The structure and thermal conductivity of each layer are given in Table 1 [11, 18, 19]. Both the quantum well layer and the DBRs layer have lateral thermal conductivity K_L and vertical thermal conductivity K_V , and for all other layers, the thermal conductivities are isotropic. Besides, the thermal conductivity of both p- and n-electrodes were assumed to be equal to the value of Au [18, 19].

III. RESULTS AND DISCUSSION

3.1 Optical Output Power and Analysis:

As shown in Figs. 3(a)-(c), the turn-on voltage was about 1.6 V. Each forward voltage was slightly increased with a further increase of the injection current. In order to verify the influence of the thermal effect on the optical output power of the array, L-I curves were tested at different heatsink temperatures. Figs. 3(a)-(c) show the L-I curves of a single LED, 3×3, and 5×5 LED array at different heatsink temperatures, respectively. Both the single LED and the array structures showed similar temperature-dependent optical properties. As shown in Fig. 3(a), the maximum optical output power of a single LED was about 2.39 mW at 50 mA. With the heating increasing under high injection

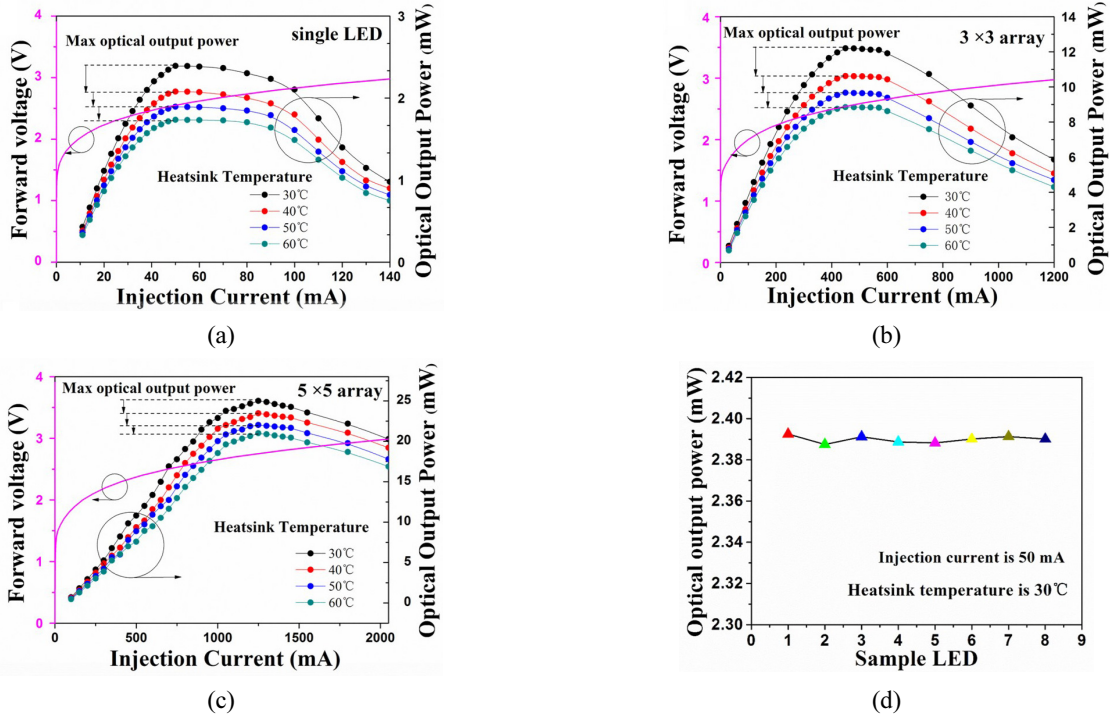


FIG. 3. (a), (b) and (c) I-V curves at 30°C, L-I curves at different temperatures of single LED and 3×3 and 5×5 LED arrays, respectively, (d) Comparison of optical output power of 8 LED pixel samples at 50 mA.

current, the optical output power was saturated and then degraded with a further increase of the injection current. The 3×3 LED array optical output power reached maximum when the injection current was about 450 mA, compared to about 1250 mA for the 5×5 array. The parallel connection of each pixel in the active matrix programmed array means that the optical output power of each pixel reached a maximum when the average injection current was 50 mA. As shown in Figs. 3(b) and 3(c), when the heatsink temperature was 30°C, the maximum optical output powers of the 3×3 and 5×5 arrays were 12.2 mW and 25.01 mW, respectively. And the maximum average optical output powers were 1.35 mW and 1 mW respectively. For a heatsink temperature of 60°C, the maximum optical output power of a single LED was 1.73 mW, and those of the 3×3 and 5×5 arrays were 8.85 mW and 21 mW, and the maximum average optical output powers were 0.98 mW and 0.84 mW, respectively. These correspond to reductions of 28%, 27% and 16% correspondingly comparing with the values at 30°C. Figure 3(d) shows the optical output power of 8 LED pixel samples at 30°C when the injection current is 50 mA. The maximum value was 2.392 mW and the minimum value was 2.387 mW, showing that the pixels were well uniformly fabricated. As the temperature increases, the quantum efficiency will decrease. The issue of optical output power droop can be described from two aspects. On one hand, the optical output power will be reduced due to the carrier leakage of the quantum wells as the temperature increases [20]. On the other hand, as the temperature increases, the defects in the material propagate quickly, which increases the non-radiative carrier recombination centers in the emission region and thus makes the internal quantum efficiency lower [11].

3.2 Junction Temperature Test and Analysis:

As it is difficult to directly measure LED chip junction temperature, the relationship between junction temperature and injection current was obtained by the wavelength peak shift method based on the temperature-dependent bandgap $[E_g(T)]$ energy. According to the equation $E_g(T) = E_g(0) - \alpha T^2 / (T + \beta)$, where positive coefficient α , β are decided by the material, the energy band gap $E_g(T)$ is a function of temperature. The energy band gap shrinks with temperature rising, and red-shift of the peak wavelength occurs while the energy band gap shrinks, according to the equation $E_g(T) = hc/\lambda$, where h is Planck constant and c is the speed of light. [11]. The peak wavelength shift method consists of a calibration measurement and a direct current measurement. The coefficient K_λ is obtained from the calibration measurement with a pulse-mode injection current. In this mode, the junction temperature is considered to be the heatsink temperature because the self-heating could be ignored. The coefficient K_λ is calculated by [10]:

$$K_\lambda = \Delta\lambda_{\text{peak}} / \Delta T \quad (6)$$

where $\Delta\lambda_{\text{peak}}$ is the variation of the peak spectrum and ΔT

is the variation of the heatsink temperature. Direct current measurement was then used to obtain the junction temperature of the LEDs. The junction temperature, T_j , was calculated by the equation [10]:

$$T_j = T_0 + \Delta\lambda / K_\lambda \quad (7)$$

where T_0 is the heatsink temperature and $\Delta\lambda$ is the change in peak wavelength between the pulsed and continuous wave modes. Figure 4(a) shows the spectra at the injection current of 20 mA under a pulsed mode with 1 μ s pulse width and 0.5% duty cycle at 30°C [10, 14]. To obtain K_λ , the wavelength peaks of each micro-LED array in the heatsink temperatures range of 20-60°C at the injection current of 20 mA are shown in Fig. 4(b). The pulse width was 1 μ s and the duty cycle was 0.5%. As the heatsink temperature increased, the peak wavelength red-shifted under the pulse mode, and K_λ were obtained by a linear fit. The value of K_λ declines as the size of the micro-LED arrays increases, and the single LED can be treated as 1×1 array. The K_λ of the single LED was 0.0563 nm/°C. And the K_λ of the 3×3, 4×4 and 5×5 arrays were 0.0519 nm/°C, 0.0478 nm/°C and 0.0441 nm/°C respectively. While changing the pulsed mode into continuous wave mode, the peak wavelength red-shifted, as shown in Fig. 4(c). The $\Delta\lambda$ and the size of the micro-LED arrays correlate positively. The $\Delta\lambda$ of the single LED was 0.191 nm at the injection current of 20 mA at 30°C, which was 2.92 nm for the 5×5 array. The thermal resistances of different LED arrays were thus obtained by Eqs. (3) and (7). As shown in Fig. 4(d), for the same dissipated heat power, the junction temperature variation rises as the size of the micro-LED arrays increases. The thermal resistance of the single LED was 39.7°C/W. And the thermal resistances of the 3×3, 4×4, and 5×5 arrays were 52°C/W, 69.7°C/W, and 84.3°C/W respectively. The differences of the thermal resistances can be explained as follows. 1) Increasing numbers of pixels leads to more heat sources, which will cause a higher ambient temperature for each pixel and increase the probability of non-radiative recombination. Thus, the pixel would produce more heat and a higher junction temperature for higher pixel numbers. 2) The reducing of the temperature difference between the internal and external pixels causes difficulty in dissipating heat. 3) Heat crosstalk is increasing with growing numbers of pixels.

The thermal crosstalk was considered for each pixel during operation. The influence of crosstalk for one pixel was maximum when all neighboring pixels were operating. The 3×3 and 5×5 arrays were used for this calculation. The junction temperature variations as a function of dissipated heat power are shown in Figs. 5(a) and (b) for the 3×3 and 5×5 arrays respectively. Thermal distributions modeled by finite element analysis are shown in the inserts of both figures. The injection current of the 3×3 array was 50 mA, while the 5×5 array's was 20 mA. The pixels of both arrays were 280×280 μ m with a pitch of 20 μ m. The calculation shows

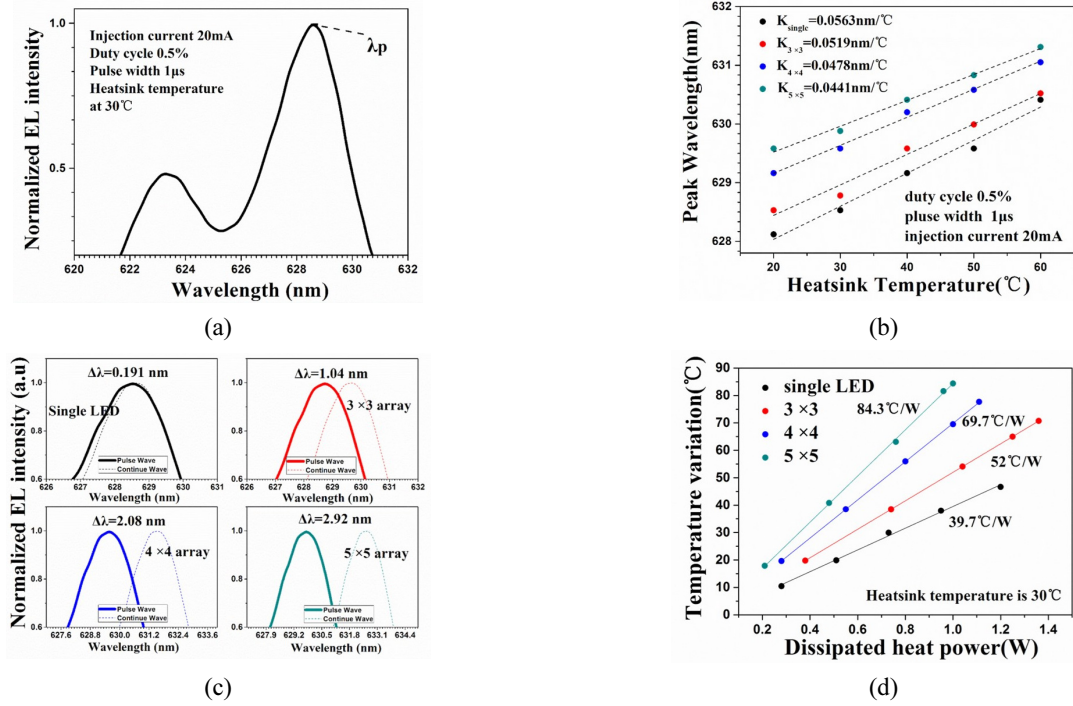


FIG. 4. (a) EL spectra at the injection current of 20mA under a pulsed mode with 1 μ s pulse width and 0.5% duty cycle at 30°C, (b) Peak wavelength shift versus heatsink temperature, (c) Comparison of the measured normalized EL intensity versus the wavelength at 20 mA under pulsed and CW modes at 30°C, (d) Thermal resistance of the single and the LED arrays at 30°C.

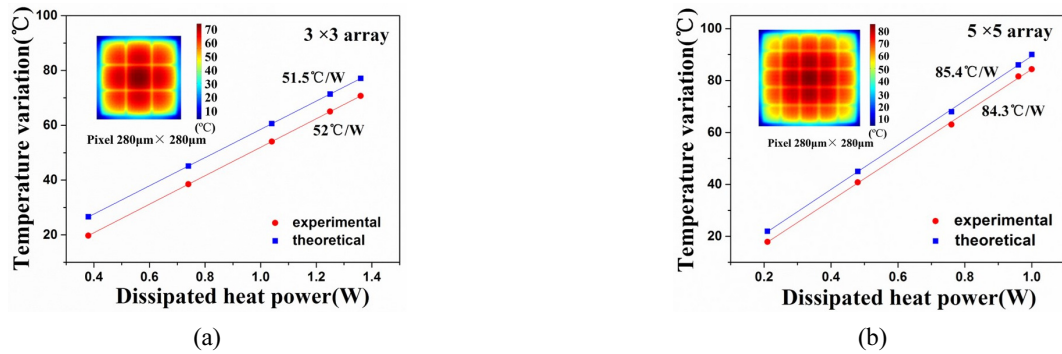


FIG. 5. Experimental and theoretical junction temperature variations as a function of dissipated heat power for the 3x3 array (a) and the 5x5 array (b).

that the center pixel has the maximum junction temperature variation. As shown in Fig. 5(a), the calculated and measured thermal resistances were 51.5°C/W and 52°C/W, respectively. Similarly, in Fig. 5(b), the calculated and measured thermal resistances were 85.4°C/W and 84.3°C/W, respectively. It is obvious that the thermal resistances obtained by calculation and measurement are consistent. In reality, the heat is dissipated by conduction, convection, and radiation. Since only thermal conduction was considered in the thermal modeling, the measured junction temperature value is greater than the calculated value.

3.3 Thermal Analysis

Enhanced heat dissipation is beneficial for improving the

optoelectronic performance of the array. The crosstalk of the center pixel is maximum when all the neighboring pixels are operating. Consequently, the 3x3 array which is the smallest array possessing a center pixel was optimum in this study. The junction temperature variations of the center pixel with different substrate thicknesses and pitches were calculated in thermal modeling, with consideration for the low thermal conductivity of the substrate and the crosstalk in the array. Figure 6(a) shows the calculated center pixel junction temperature variations of the 3x3 array as a function of separation distance under different injection currents during continuous operation at 30°C. The junction temperature variation of the center pixel was determined to be 78.7°C at 50 mA with a pitch of 10 μ m. And it was

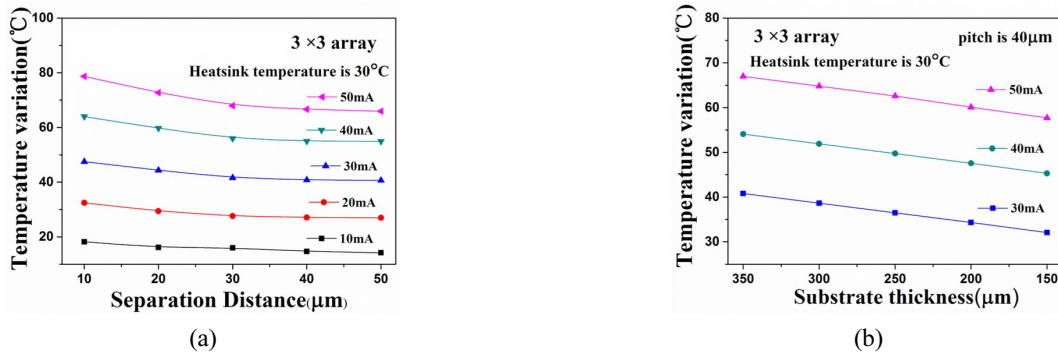


FIG. 6. (a) Center pixel junction temperature variation of the 3×3 array as a function of separation distance at different injection currents; (b) Center pixel junction temperature of the 3×3 array as a function of substrate thickness at different injection currents with a pitch of 40 μm.

reduced to 66.0°C for a pitch of 40 μm and 65.9°C for the pitch of 50 μm at 50 mA. No further decrease was observed with larger values of pitch. Additionally, when increasing the injection current for a pitch of 10 μm, the values were 18.3°C and 64.5°C at 10 mA and 40 mA, respectively. The junction temperature variation was not obviously influenced by the crosstalk for pitches greater than 40 μm. Thus, the anticorrelation between the temperature and the separation distance may be due to the interference heating effects. Figure 6(b) shows the calculated center pixel junction temperature variation of the 3×3 array as a function of substrate thickness for different injection currents with a pitch of 40 μm at 30°C. The junction temperature variation of the center pixel decreases with reducing substrate thickness for the same injection current. Most of the generated heat spill into the heatsink through the substrate. Thus, the LED with thinner substrate has better heat removal capability because of shorter heat transfer time. To satisfy the fabrication condition, the substrate thickness should be no less than 150 μm. Meanwhile, the pitch was chosen to be 40 μm.

IV. CONCLUSION

In this study, we have shown the thermal, electrical, and optical properties of 3×3, 4×4, and 5×5 LED arrays fabricated using a new method based on the Micro-Opto-Electro-Mechanical Systems (MOEMS) integrated technique. As the number of array pixels and heatsink temperature increase, the photoelectric properties of the pixels decrease and the pixel thermal resistance increases. The junction temperature of the center pixel is maximum owing to thermal crosstalk from neighboring pixels. The substrate thickness and pixel separation pitch were optimized to enhance LED array heat dissipation by thermal modeling. The optimal values were found to be an array pixel pitch of 40 μm and 150 μm substrate thickness.

ACKNOWLEDGMENT

This work was supported by the National Natural Science Foundation of China (NSFC) under grant no.61274122, the Jilin Province and Technology Development Plan under grant no.20100351 and 20120323, the Changchun Science and Technology Plan under grant no.2013269, and the Youth Innovation Promotion Association of CAS under grant no.2014193.

REFERENCES

1. S. H. Lee, K. J. Chang, G. T. Hwang, and K. J. Lee, "Self-powered flexible inorganic electronic system," *Nano Energy*, **14**, 111-125 (2014).
2. J. Day, J. Li, D. Y. C. Lie, C. Bradford, J. Y. Lin, and H. X. Jiang, "III-Nitride full-scale high-resolution microdisplays," *Applied Physics Letters*, **99**, 031116 (2011).
3. X. Li, J. D. Budai, and J. Y. Howe, "New yellow Ba_{0.93}Eu_{0.07}Al₂O₄ phosphor for warm-white light-emitting diodes through single-emitting-center conversion," *Light Science & Applications*, **2**, 50 (2013).
4. E. Matioli, S. Brinkley, K. M. Kelchner, Y. L. Hu, S. Nakamura, S. Denbaars, J. Speck and C. Weisbuch, "High-brightness polarized light-emitting diodes," *Light Science & Applications*, **1**, 479-482 (2012).
5. Z. J. Liu, K. M. Wong, W. K. Chi, C. W. Tang, and K. M. Lau, "Monolithic LED microdisplay on active matrix substrate using flip-chip technology," *IEEE Journal of Selected Topics in Quantum Electronics*, **15**, 1298-1302 (2009).
6. Y. C. Chu, M. H. Wu, C. J. Chung, Y. H. Fang, and Y. K. Su, "Micro-chip shaping for luminance enhancement of gan micro-light-emitting diodes array," *Electron Device Letters IEEE*, **35**, 771-773 (2014).
7. A. L. Chaudet, M. Neil, P. Degenaar, K. Mehran, R. Berlinguer-Palmini, B. Corbet, P. Maaskant, D. Rogerson, P. Lanigan, E. Bamberg, B. Roska, "Development of optics with micro-LED arrays for improved opto-electronic neural stimulation," *Proceedings of SPIE - The International Society for Optical Engineering*, **8586**, 455-464 (2013).
8. Q. Shan, Q. Dai, S. Chhajed, J. Cho, and E. F. Schubert,

- "Analysis of thermal properties of GaInN light-emitting diodes and laser diodes," *Journal of Applied Physics*. **108**, 084504 (2010).
9. J. Herrmsdorf, J. J. D. Mckendry, S. Zhang, and E. Xie, "Active-matrix GaN micro light-emitting diode display with unprecedented brightness," *IEEE Transactions on Electron Devices*. **62**, 1 (2015).
 10. M. S. Kim, H. K. Lee, and J. S. Yu, "Device characteristics and thermal analysis of AlGaInP-based red monolithic light-emitting diode arrays," *Semiconductor Science & Technology*. **28**, 348-354(2013).
 11. H. K. Lee, D. H. Lee, Y. M. Song, Y. T. Lee and J. S. Yu, "Thermal measurements and analysis of AlGaInP/GaInP MQW red LEDs with different chip sizes and substrate thicknesses," *Solid-State Electronics*. **56**, 79-84 (2011).
 12. C. Tian, W. Wang, J. Liang, Z. Liang, Y. Qin, and J. Lv, "Theoretical and experimental analysis of AlGaInP micro-LED array with square-circle anode," *Aip Advances*. **5**, 771 (2015).
 13. X. Bao, J. Liang, Z. Liang, W. Wang, C. Tian, Y. Qin, and J. Lv, "Design and fabrication of AlGaInP-based micro-light-emitting-diode array devices," *Optics & Laser Technology*. **78**, 34-41 (2016).
 14. K. Chen and N. Narendran, "Estimating the average junction temperature of AlGaInP LED arrays by spectral analysis," *Microelectronics Reliability*. **53**, 701-705 (2013).
 15. R. J. Cheng and K. M. Liew, "A meshless analysis of three-dimensional transient heat conduction problems," *Engineering Analysis with Boundary Elements*. **36**, 203-210 (2012).
 16. Y. S. Muzychka, M. M. Yovanovich, and J. R. Culham, "Thermal spreading resistance in compound and orthotropic systems," *Journal of Thermophysics & Heat Transfer*. **18**, 45-51 (2004).
 17. M. M. Yovanovich, Y. S. Muzychka, and J. R. Culham, "Spreading resistance of isoflux rectangles and strips on compound flux channels," *Journal of Thermophysics & Heat Transfer*. **13**, 495-500 (1999).
 18. Wlodzimierz and Nakwaski, "Thermal conductivity of binary, ternary, and quaternary III-V compounds," *Journal of Applied Physics*. **64**, 159 (1988).
 19. M. Guden and J. Piprek, "Material parameters of quaternary III-V semiconductors for multilayer mirrors at 1.55 μm wavelength" *Modelling and Simulation in Materials Science and Engineering*. **4**, 349-357 (1996).
 20. M. F. Schubert, J. Xu, J. K. Kim, E. F. Schubert, M. H. Kim, S. Yoon, S. M. Lee, C. Sone, T. Sakong, and Y. Park, "Polarization-matched GaInN/AlGaInN multi-quantum-well light-emitting diodes with reduced efficiency droop," *Applied physics letters* **93**, 041102 (2008).